Journal of Alloys and Compounds 834 (2020) 155003

Contents lists available at ScienceDirect

Journal of Alloys and Compounds

journal homepage: http://www.elsevier.com/locate/jalcom

Investigating the thermal stability of the chemical vapour deposited zirconium carbide layers

Saphina Biira [a, *], T.T. Thabethe [b], T.T. Hlatshwayo [b], H. Bissett [c], T. Ntsoane [c], J.B. Malherbe [b]

[a] Department of Physics, Busitema University, Tororo, Uganda
[b] Department of Physics, University of Pretoria, Pretoria, South Africa
[c] South African Nuclear Energy Corporation, Pretoria, South Africa

ARTICLE INFO

Article history:
Received 4 July 2019
Received in revised form
29 March 2020
Accepted 30 March 2020
Available online 8 April 2020

Keywords:
Annealing temperature
Chemical vapour deposition
ZrC layers
Microstructural properties
Surface morphology

ABSTRACT

The effect of thermal treatment on zirconium carbide (ZrC) layers deposited by chemical vapour deposition process was investigated using X-ray diffraction (XRD), Raman spectroscopy, nanoindention and scanning electron microscopy (SEM). The ZrC layers deposited at 1400 °C (composed of 96% ZrC and 4% C) were annealed at 1500, 1600, 1700 and 1800 °C for 2 h under high vacuum of 2.6×10^{-7} mbar. After annealing, the lattice constant and the average crystallite sizes were found to increase whereas the lattice strain and dislocation density decreased. The preferred orientation of the as-deposited layers was (220); it changed to (200) when annealed at 1500 °C and 1600 °C. At annealing temperature of 1700 °C and 1800 °C, the preferred orientation was (220) just like for the as-deposited ZrC layers. From Raman spectroscopy analysis, the I_D/I_G ratio reduced from 0.694 to 0.414 with annealing temperature indicating an improvement in crystallinity level and a decrease in the defects in the carbon material in the ZrC layers. The hardness of the layers was found to decrease slightly with annealing temperature from 26.4 ± 0.6 GPa to 21.3 ± 0.5 GPa. Some voids initially present in the as-deposited ZrC layers closed up and particles increased in size with annealing temperature.

1. Introduction

Over the past decades, refractory metal carbides have attracted attention because of their wide range of applications that is attributed to their excellent properties [1]. ZrC being one of the refractory compounds is characterised by high hardness, high thermal and electrical conductivities, chemical inertness, low neutron capture cross section and high melting temperature (over 3500 °C) [1,2]. This unique combination of ZrC properties has found importance in technical applications such as cutting tools and in the form of thin heat and wear-resistant coatings [2,3]. Additionally, ZrC has attracted attention as a component of diffusion barriers for fission products in the nuclear tri-structural isotropic (TRISO) fuel particle [4,5], most especially in the Generation IV high temperature nuclear reactors [6]. The Generation IV high temperature nuclear reactors are designed to reach a maximum temperature of 1500 °C and beyond. High temperatures improve thermal efficiencies, hence more electricity output per unit of nuclear fuel [7]. A number of studies have been conducted on preparation and characterisation of ZrC films, but obtaining ZrC films of desired properties for nuclear applications has remained a challenge. This is due to variation of ZrC stoichiometry and properties with preparation techniques. Of the many techniques for the preparation of ZrC layers, chemical vapour deposition (CVD) is the preferred technique over other techniques. Since it can produce films with good layer uniformity and purity [5]. However, the CVD growth of ZrC layers free of carbon inclusions and sometimes oxygen is very difficult. Free carbon and oxygen act as impurities and therefore affect the properties of ZrC produced [8,9]. The ZrC layers deposited at about 1400 °C were reported to possess good mechanical, morphological and compositional characteristics [10]. If these ZrC layers are used as one of the coating layers of the nuclear TRISO fuel particle for the Generation IV high temperature nuclear reactors, it will be subjected to high temperature even up to 1800 °C. Studies have reported that it is hard to grow carbon free ZrC layers by CVD [11,12] and indeed in most of the experiments we have conducted, traces of carbon have

* Corresponding author.
E-mail address: bsaphina@yahoo.co.uk (S. Biira).

https://doi.org/10.1016/j.jallcom.2020.155003
0925-8388/

always shown up [8,9]. This is disadvantageous; the presence of carbon inclusions in the ZrC layers affect its mechanical strength, oxidation and irradiation resistance [5]. Since traces of carbon inclusions are hard to eliminate during ZrC layers growth by CVD, the thermal behaviour of carbon inclusions in conjunction with ZrC should be investigated. Therefore, in this work we investigate the thermal stability of ZrC layers (with traces of carbon inclusions) in relation to surface morphology, structure properties and hardness.

2. Experimental

2.1. ZrC deposition and annealing process

The ZrC layers were deposited on graphite substrates (of diameter 10 mm and thickness of 2.5 mm) in a vertical wall chemical vapour deposition (CVD) reactor. The deposition was conducted at 1400 °C for 2 h with the CVD system pressure maintained at atmospheric pressure. The ZrC layers were produced by the reaction of zirconium tetrachloride ($ZrCl_4$) and methane in the presence of hydrogen and argon in a vertical graphite tube as the reaction chamber. The flow rates of methane, hydrogen and argon were measured by rotameters. The $ZrCl_4$ powder was kept at 300 °C throughout the experimental running time so as to maximise and control its vapour pressure. The details of the deposition process have been described in Ref. [8,13]. The as-deposited ZrC layers at 1400 °C were composed of 96% ZrC and 4% C. The phase composition of the deposited layers was analysed by the Rietveld refinement method using the TOPAS V4.2 [14] software package from the XRD data. The thickness of the deposited ZrC layer was estimated to be 28 ± 2 μm. It was calculated from the mass increase of the substrate before and after deposition, the theoretical density of ZrC and surface area of the coated surface of the substrate.

The as-deposited ZrC layers were placed in the glassy carbon crucibles and annealed in an automated Webb 77 graphite furnace. The as-deposited ZrC samples were annealed at four different temperatures (i.e. 1500 °C, 1600 °C, 1700 °C and 1800 °C) at a holding time (annealing/heating time at a particular temperature) of 2 h for each sample. The chosen annealing temperatures were higher than the preparation temperature. This was done so as to observe the changes at higher temperatures. During annealing, the furnace environment consisted of high vacuum in the range of 10^{-7} mbar. After annealing the furnace was cooled down at a cooling rate of 20 °C/min to room temperature before the samples were removed.

2.2. Characterisation

X-ray diffraction (XRD) analysis was used to determine the crystal structure and orientation of the deposited and annealed zirconium carbide layers. This was carried out using a Bruker XRD D8 Advance with a Cu K_α radiation source ($\lambda = 1.54056$ Å) within the recording range of 15° to 125° and a step size of 0.04. The working potential and the corresponding current used during spectrum acquisition were 40 kV and 40 mA respectively. The top surfaces of the samples were mounted horizontally flat in the sample holders. Measurements were done in reflection geometry with the incident beam irradiating the samples at the geometrical centre covering almost the whole geometry of the top surface of the ZrC samples, hence improving statistical reliability of the data collected. Diffracted data were collected using a LynxEye position sensitive detector.

A Zeiss Ultra Plus Field Emission-Scanning Electron microscopy (FE-SEM) was used to characterise the surface morphology of the layers at an acceleration voltage of 1 kV. The as-deposited and annealed ZrC layers were also characterised by Raman spectroscopy. The Raman spectroscopy analysis (Horiba Jobin Yvon) was performed using an Ar–Kr laser with an excitation wavelength of 514 nm and laser power of 1.48 mW. The Raman spectra were acquired from 200 cm^{-1} –1800 cm^{-1} at an aperture of 50× the objective lens. The hardness of the ZrC layers was determined using a nanoindeter with a load of 10 mN. For each sample five indentations were made at different points on the sample and the average was taken.

3. Results and discussion

3.1. Microstructure and phase composition (XRD)

Fig. 1 gives the XRD spectra for the samples annealed at different temperatures (i.e. 1500 °C, 1600 °C, 1700 °C and 1800 °C). The XRD pattern of the as-deposited sample (indicated by 1400 °C because the layer was grown at this temperature) was included for comparison purposes. The as-deposited and annealed samples showed the presence of (111), (200), (220), (311), (222), (400), (331), (420), (422) and (511) reflections at 2θ° of about 32.9, 38.3, 55.2, 65.9, 69.2, 81.9, 91.2, 94.3, 106.8 and 116.8 respectively when matched with the standard ICDD (International Centre for Diffraction Data Released 2007) file numbers ZrC: 03-065-8833. Some traces of a carbon phase were also revealed when matched with the ICDD file number C: 00-008-0415, with the most prominent peak (represented by C in Fig. 1) at reflection (hkil) of (0002) corresponding to 2θ° at about 26.5. Therefore, the XRD pattern was composed of ZrC and some traces of carbon phase which emerged as the annealing temperature increased. By inspecting the XRD patterns, the annealed samples had increased peak intensities and narrowed peak width as compared to the as-deposited sample. This implies that the level of crystallinity of the samples improves and the crystallite sizes grow larger, whereas the strain in the layer reduces. The effect of annealing temperature on crystallite sizes of and strain in the ZrC samples are discussed in Subsection 3.1.1 and 3.1.2 respectively. The traces of free carbon which were originally co-deposited with ZrC sample continued to emerge, with its peaks' full width at half maxima (FWHM) decreasing as the annealing temperature increased (see Section 3.2). It is important to note that

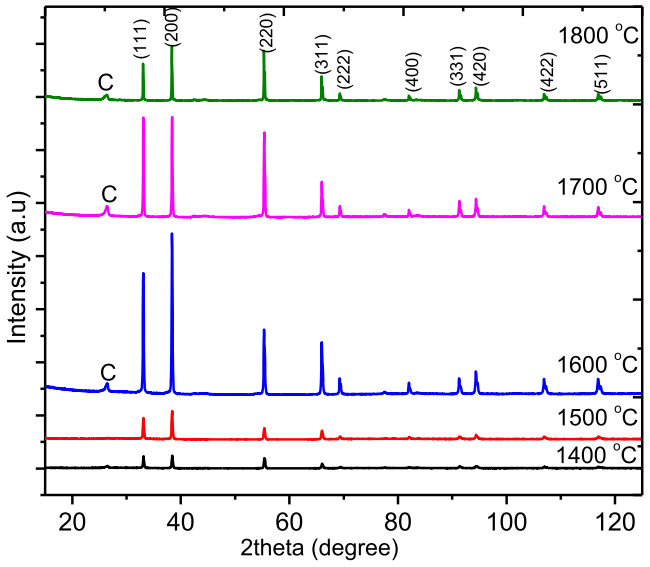

Fig. 1. XRD pattern of ZrC layers annealed at different temperatures.

ZrC and graphite have their melting temperatures close to each other (i.e. both graphite and ZrC melts above 3500 °C) [1].

3.1.1. Average crystallite size, lattice parameter and preferred orientation

The average crystallite size and lattice strain were determined from the full width at half maximum (FWHM) or broadening of the first five XRD peaks. In general, peak broadening of an XRD peak is caused by three factors: (1) crystallite size, (2) instrumental broadening and (3) the presence of strain in the material. After subtracting the instrumental broadening, peak broadening was used to determine crystallite size and the strain in the material. This is because peak broadening decreases with increase in the crystallite sizes and increases with an increase in strain [15]. In this study, to subtract the peak broadening due the instrument the XRD pattern of the NIST standard material (Al_2O_3) was collected (which has a high level of crystallinity and very sharp Bragg peaks). The same optical configurations that were used for the Al_2O_3 sample were also used to obtain the XRD pattern of the ZrC samples. This diffractogram of this standard sample was used for determination of the peak broadening which comes from the instrument slits etc. Then we carried out a deconvolution of the XRD obtained from the as-deposited and annealed ZrC samples. So that the XRD data used is free from instrumental broadening.

The contributions of strain ε and crystallite size D to peak broadening (i.e. B_ε and B_D respectively) do not depend on one another. It has been reported that crystallite sizes are best approximated by the Cauchy distribution, whereas microstrain (lattice distortions) is best appoximated by a Gaussian distribution. Therefore, peak broadening may be given by either $B = B_D + B_\varepsilon$(Cauchy) or $B = B_D{}^2 + B_\varepsilon{}^2$ (Gauss) [16,17]. It has been reported that in thin films the contribution to peak broadening due to crystallite size is much greater than that from microstrain. Therefore, the Cauchy distribution is usually a better fit for peak broadening than Gaussian [16].

The overall peak broadening is then given by combining Equations $B = \frac{K\lambda}{D\cos\theta_B}$ (Scherrer's formula) and $B = 4\varepsilon\tan\theta$ [18] as given in Equation (1)

$$B = 4\varepsilon\tan\theta + \frac{K\lambda}{D\cos\theta} \tag{1}$$

Rewriting Equation (1), we get the Williamson-Hall Equation (2):

$$B\cos\theta = 4\varepsilon\sin\theta + \frac{K\lambda}{D} \tag{2}$$

To compensate for the peak shape, a constant K called the shape factor was introduced, which is usually about 0.94 as derived by Scherrer for cubic structures [19]. Equation (2) was plotted with $B\cos\theta$ on the vertical axis and $4\sin\theta$ on the horizontal axis, so that strain could be determined from the slope of the graph and the average crystallite size from the vertical intercept [18,20].

The sizes of crystallites in polycrystalline materials have significant effects on its properties. For instance, decreasing the crystallite size increases the hardness and strength of the material [21]. Therefore, it is important to determine the crystallite sizes of the materials prepared. In this case, the average crystallite sizes of ZrC increase from 44.8 ± 0.5 nm to 88.5 ± 0.9 nm when the annealing temperature is increased from 1400 °C (as deposited) to 1800 °C as indicated in Fig. 2. The increase in crystallite size as annealing temperature is increased may be resulting from Ostwald ripening and grain boundary migration as illustrated in Fig. 3. At room temperature the grain boundaries are almost static; when the temperatures are increased the grain boundaries are set in motion

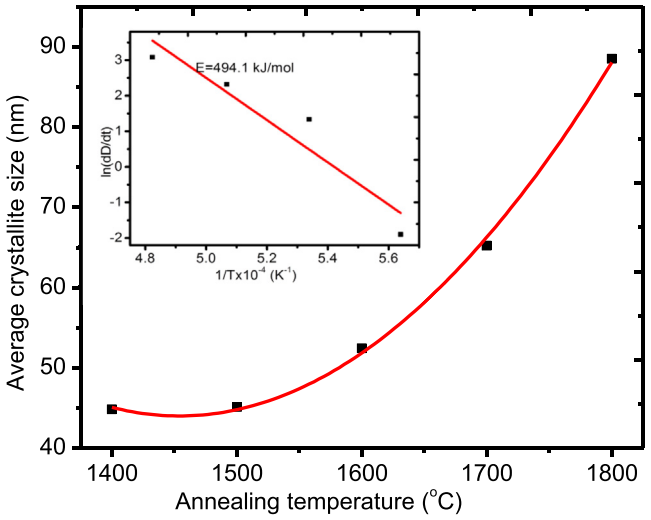

Fig. 2. Dependence of average crystallite growth on annealing temperature.

(grain boundary migration). The grain boundary migration causes the thickening of crystallite structures (due to the combining of boundary boundaries), thereby causing increase in crystallite size. The occurrence of grain boundary migration during annealing of films or layers results into a reduction of the total grain boundary distribution which in turn decreases the grain boundary energy. Reduction of grain boundary energy enhances crystallite growth; therefore, increasing the annealing temperature increases the driving force for the crystallite growth [22]. Crystallite growth with temperature is in such a way as to reduce the total Gibbs free energy of the system in attempt to attain equilibrium condition (small crystallite have high surface energy). Here a number of other factors are involved (i.e. minimisation of the surface, interface and strain energies between different oriented grains) which can result in an Ostwald ripening process where the larger crystals grows preferentially and the smaller ones are swallowed up [23]. This parasitic growth of the crystals maximises the areas of crystal planes with lower surface energies also in line with Wulf's law [24].

Assuming Arrhenius law (i.e. $\frac{dD}{dt} = k_o\exp\left(\frac{-E}{RT}\right)$) applies for crystallite growth during annealing, a plot of $ln(dD/dt)$ against $1/T$ is shown in Fig. 2 (insert). In this case dD/dt is the crystallite growth rate at various annealing temperatures, E is the activation energy for crystallite growth, T is the annealing temperature, R the gas constant and k_o is the pre-exponential constant [22]. The relationship between $ln(dD/dt)$ and $1/T$ is linear and its slope is used to obtain the value of E. In this study, the value of $E = 494 \pm 50$ kJ/mol is reported, this value is higher than the one reported by Wang et al. (2008) of 305 kJ/mol for ZrC crystal growth from CH_4 and $ZrCl_4$ [25]. Generally, there is no limit for activation energy; if the activation energy is sufficiently large it means reaction is slow. Therefore, the higher the activation energy, the harder is for the crystallite size to increase. From the value of activation energy obtained in this study, we can therefore conclude that the crystallite growth was restricted. Although the increase in average crystallite sizes is observed, the possibility of crystal growth retardation may therefore not be dismissed. This might have resulted from the presence of carbon inclusions in the ZrC layer. The carbon inclusions (impurities) in the ZrC layer may influence the pinning of the grain boundary migration and grain boundary grooving at the free surface of the thin film [26]. This is because the rate of ZrC grain boundary migration may partly be controlled by the diffusion rate of the carbon inclusions.

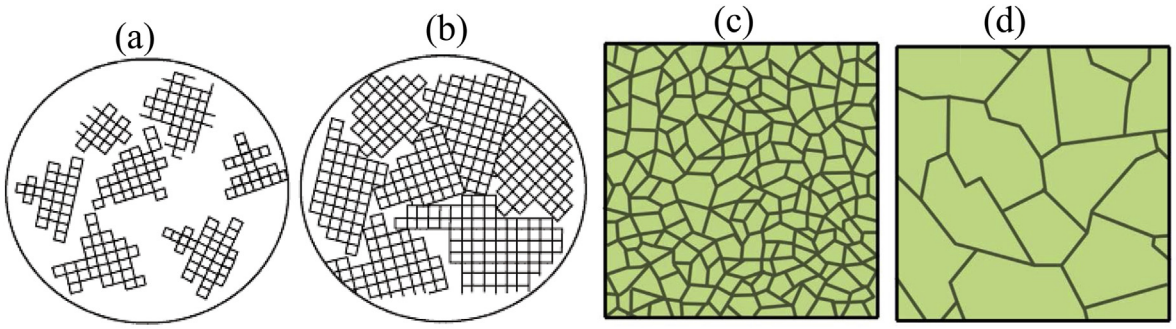

Fig. 3. (a)–(b) illustrates the change in preferred orientation growth and rearrangement of crystal plane and while (c) to (d) illustrates the crystallite growth and grain boundary migration when the annealing temperature is increased respectively.

A decrease in the diffraction angles of both ZrC and carbon peaks as the annealing temperature was increased was observed. The decrease in diffraction angles is an indication that the lattice parameter of ZrC increased with annealing temperature. To confirm this, the lattice parameters of ZrC were calculated from the XRD spectra using the first five peaks in the patterns. The Nelson-Riley plots were used to minimise errors so as to obtain the corrected values of the lattice parameter [9]. The graph presenting the calculated lattice parameters against the Nelson-Riley function $f(\theta)$ is plotted as shown in Fig. 4. The extrapolated value at the y-axis was considered as the desired lattice parameter values for each annealing temperatures. It can be observed that there is a slight increase in lattice parameter values as the annealing temperature is increased (i.e. from 4.6912 ± 0.0005 Å for as-deposited samples to 4.6954 ± 0.0004 Å for sample annealed at 1800 °C). The increase in lattice parameter values with annealing temperature may be resulting from lattice slackening and increased crystallite sizes of both ZrC and C. Otherwise one would expect the decrease in lattice parameter as annealing temperature is increased due to reduced defects in the lattice structure. Generally, when the annealing temperature is increased, the lattice parameters are increased due to the materials expansion. However, there are always a number of defects in coatings deposited by CVD, during annealing these defects may decrease (due to defect migration and sintering effect) and the lattice is decreased. As a result of these competing processes, the change in lattice parameter may be reduced.

Fig. 5 shows the variation of texture coefficient with annealing temperatures. Preferred orientation is obtained by texture analysis. There are mainly two ways of determining preferred orientation; either in terms of pole figures (by using any of omega and chi curves measurements) and or texture coefficients [21,27]. In this study, the texture coefficient method was applied. The texture coefficient $T(hkl)$ for each of the first five diffraction peaks in the ZrC films was calculated from their intensities relative to each other and to the standard powder pattern (International Centre for Diffraction Data (ICDD) file number ZrC: 03-065-8833) by applying the Harris method with the help of equation (3) [21,28].

$$T(hkl) = \frac{I(hkl)/I_0(hkl)}{(1/N)\sum_N I(hkl)/I_0(hkl)} \quad (3)$$

where $I(hkl)$ is the relative intensity of the (hkl) plane as measured from the diffraction pattern of the sample and $N$is the number of diffraction peaks considered. The quantity $I_0(hkl)$ is the relative integrated intensity reference of the randomly oriented grains (powder of the sample). The value of $I_0(hkl)$ for the corresponding plane was obtained from the ICDD data file number ZrC: 03-065-8833. It can be observed that the crystallographic planes of the ZrC layers have certain preferred orientations that develop during deposition and subsequently during heat treatment. This means that the layer crystallite growth process is selective in terms of

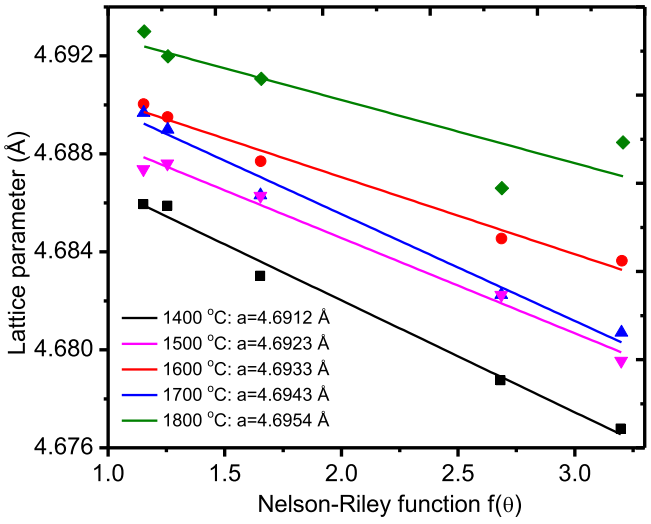

Fig. 4. The plots of the apparent lattice parameters as a function of the Nelson-Riley function at different annealing temperatures.

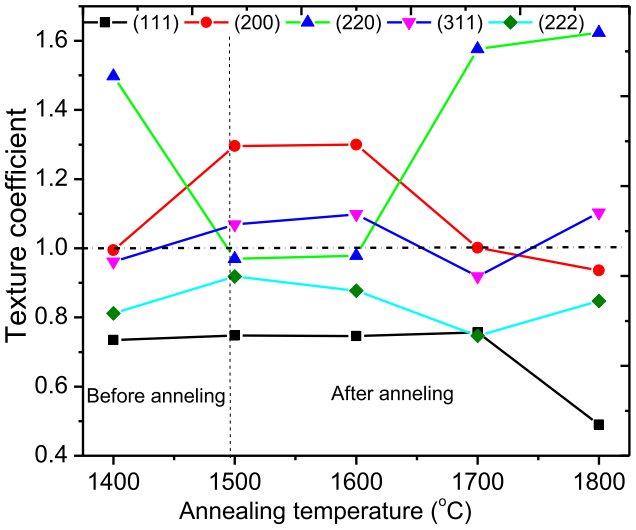

Fig. 5. Variation of texture coefficient with annealing temperature.

crystal plane orientations. Increasing annealing temperature increases the crystal growth kinetics. Due to the anisotropy in crystals they always grow at different rates along different directions because of the differences in attachment energy for the different crystal planes. The as-deposited ZrC layers showed a (220) plane as the preferred orientation. However, when annealed at temperature 1500 °C and 1600 °C, (200) and (311) emerged as the preferred planes. When the samples were further annealed at 1700 °C and 1800 °C, the planes (220) resurfaced again as the preferred orientation. At all the temperatures the intensity of (111) peak was fairly strong, however in comparison with the intensities of the random ZrC powder of the standard data, (111) was the least preferred orientation. The change in crystallographic orientations may be explained by the minimisation of total free energy.

Crystallite growth involves the minimisation of total free energy. The total free energy is the sum of strain energy, surface energy and grain interface energy. This means crystallites with higher surface energy were consumed into the neighbouring crystallites according to Wulf's law [24] as illustrated in Fig. 3. This decreases the total surface energy. This explains the change of preferred orientation from (220) (as deposited sample) to (200) for annealing temperatures of 1500 °C and 1600 °C.

At 1700 °C and 1800 °C there was a rapid increase in crystallite growth, this means that the dominant controlling factor for the crystallite growth was the minimisation of strain energy. It has been reported that, the crystallographic plane (220) has the lowest plastic strain energy for face-centred cubic materials [29]. This explains the re-emerging of (220) at higher annealing temperatures.

Preferred orientation is also driven by the interaction (and interface strain energy) between the growing thin film and the graphite substrate. This is even outstanding for very thin films. Therefore, the influence of the substrate on the preferred orientation is likely to be minimal for the as-deposited ZrC layer of 28 ± 2 μm thickness. During annealing, it was anticipated that the deposited layer had more effect on the final microstructure layer than the substrate, since the layer is not 'perfect' as compared to the substrate.

3.1.2. Lattice strain and dislocation density

The concentration of defects in the structure of the samples was examined by calculating the values of lattice strain (ε) and dislocation density (ρ). As already stated, the lattice strain was determined from equation (2) [18,19].

The dislocation density has been defined as the total length of all the dislocation lines per unit volume of a crystalline material [30]. Taking the crystallite size as the cube root of the crystallite volume and assuming all the crystallites have the same size and shape, the relationship between δ and D can be expressed as given in Equation (4) [16]:

$$\rho = \frac{nD}{D^3} = \frac{n}{D^2} \tag{4}$$

where n is number of dislocation lines in a unit volume of the crystallite. Assuming a random distribution of dislocations, the number of dislocation lines crossing a unit area in the layer of the as-deposited and annealed ZrC layers was calculated from Williamson-Smallman's formula [16,30] given by Equation (4)

$$\rho = \frac{1}{D^2} \tag{5}$$

Since the as-deposited and annealed ZrC layers were ultrathin compared to the thickness of the graphite substrate, then the deposited layers are exposed to some level of strain originating from the (i) densification of the layers, (ii) differences in the thermal expansions between the substrate and the layer and (iii) intrinsic strains [29]. Dislocation density is the total length of dislocation lines per unit volume of the crystal [30,31]. Fig. 6 represents the variation of lattice strain and dislocation density with annealing temperatures. The calculated dislocation values decreased with increase in annealing temperatures. Since dislocations are regions in the crystal structure where the atoms are not orderly aligned, therefore dislocations are also a category of defects in crystals. This means that the decrease in dislocation density decreases the level of defects in the ZrC layer. As already explained in Subsection 3.1.1 that during crystallite growth there is reduction of total grain boundaries, the fewer the grain boundaries the lesser the material is strained [32]. Grain boundaries are also a form of defects in a material (planar defects) since atoms neighbouring the grain boundary in some cases do not perfectly follow the crystalline arrangement. Therefore, annealing the material enhances recovery which reduces strain in the material lattice. To improve on the reliability of these results it would be important to compare them with an alternative and independent determination of the dislocations such as TEM images, this has not been provided in this study.

3.2. Raman spectroscopy analysis

Raman spectroscopic analysis produce a characteristic spectrum for materials depending on the vibrational modes of their molecules [33]. Fig. 7 shows the Raman spectra obtained at room temperature from (a) the graphite substrate and from (b) the ZrC samples annealed for 2 h at different annealing temperatures. Within the spectral range the ZrC samples revealed only the D and G peaks observed and no peaks of ZrC were observed. This is attributed to the fact that ZrC does not have active vibrational modes detectable by Raman spectroscopy. It is also an indication that no carbon vacancies were detected in all the samples [34,35], instead the samples before and after annealing revealed the presence of free carbon (evidenced by the presence of D and G-band). The observed D and peaks cannot be originating from the graphite substrate since the D and G peaks from the graphite substrate are sharp and narrow as shown in Fig. 7(a). Besides, the thickness of the as deposited layer is 28 ± 2 μm, which is much greater than the depth of penetration of the 514 nm laser into the ZrC layer. The D-band is associated with the defect concentration or measure of disorders in the C—C bonds within graphitic materials. The G-band

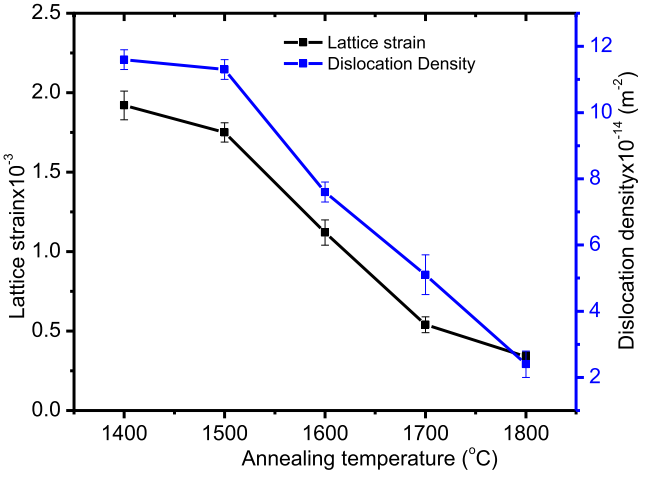

Fig. 6. Effect of annealing temperature on the lattice strain and dislocation density.

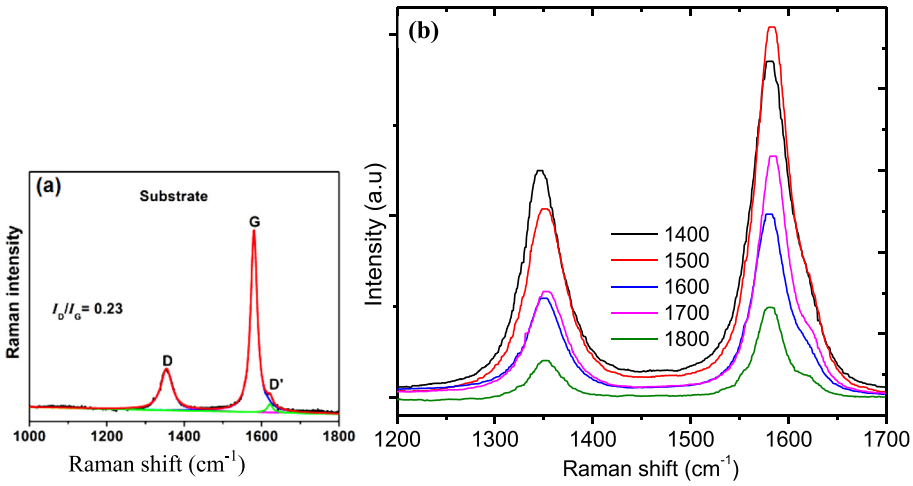

Fig. 7. The Raman spectra **(a)** of the graphite substrate and **(b)** of ZrC layers annealed at different annealing temperatures.

is associated with in-plane vibrations of C–C bonds and is a measure of graphitization or degree of metallicity of graphitic materials [36]. There was increase in the peak intensities of both D and G peaks as the annealing temperature increased. This may be due to movement of C to the near surface of the sample. Also, as the annealing temperature increased from 1500 °C to 1800 °C there was a shift and narrowing of both the D and G peaks. The D and G peaks shifted from 1343 to 1345 cm^{-1} and from 1579 to 1582 cm^{-1} respectively. The full width at half maxima (FWHM) of D and G peaks changed from 50.32 to 45.7 cm^{-1} and 50.63 to 37.96 cm^{-1} respectively (see Fig. 8).

The shift in peak position and the narrowing of the peaks shows that there is a decrease in the level of defects in the carbon materials just as in the ZrC material as the annealing temperature is increased. The intensity of the D-band (I_D) decreased while that of the G-band (I_G) increased as the annealing temperature increased. The values of I_D/I_G decreases with increase in annealing temperature as shown in Fig. 8. The I_D/I_G ratio is a measure of the presence of defects in the structure of the carbon materials. It has been reported that the G peak results from the in-plane vibrations of sp^2 bonded carbon atoms while the D peak is caused by out of plane vibrations due to the presence of structural defects [37,38]. This means that I_D/I_G forms a connection with sp^3/sp^2 ratio. As the annealing temperature was increased, there was increased transition from sp^3 material to sp^2 material, meaning that there was a reduction in the defects in the structure of the carbon material [37]. So the free carbon in the deposited layers becomes more graphitic. This is supported by the corresponding decrease in the FWHM peak widths of the G peak as already shown in Fig. 8.

The peak G position of the annealed samples increased with temperatures as seen in Fig. 7. This means that thermal treatment of the samples resulted into some degree of recovery of the carbon structure (from amorphous carbon to graphitic carbon). In Fig. 8, the FWHM of the annealed samples at different temperatures were compared to the FWHM of the G peak for the as deposited sample. The results showed that the FWHM of the G peak narrowed, implying increased degree of crystallisation of the carbon material in the layers [37] with annealing temperature.

It has been reported that the extra carbon in ZrC can alter the oxidation behaviour of ZrC materials [5]. The extra carbon can increase the production of CO_2 which may increase the chances of inter-crystalline fracture and below normal temperature fracture. It can also change the materials response to temperature in terms of thermal expansion which can results into cracks, hence reducing its strength.

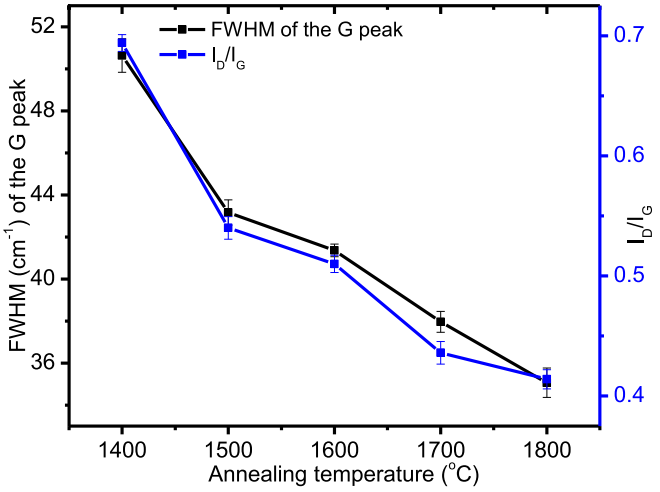

Fig. 8. Variation of FWHM of the G peak and I_G/I_D with annealing temperature.

3.3. Hardness measurements

It is important to establish the hardness of a material processed because, hardness has a direct bearing on the material strength, wear resistance and other properties. The Vickers hardness value of the as-deposited ZrC layer (at a temperature of 1400 °C) was 27.6 ± 0.4 GPa. After annealing the samples at temperatures of 1500 °C, 1600 °C, 1700 °C, and 1800 °C the hardness values were found to be 26.4 ± 0.6 GPa, 24.0 ± 0.4 GPa, 22.9 ± 0.3 GPa and 21.3 ± 0.5 GPa respectively. As already observed in Section 3.1.1, increasing annealing temperature increases the diffusion based crystallite growth. According to the Hall-Petch relation [39], a decrease in material strength is therefore expected and consequently a decrease in the hardness of the material. There is also increased amount of free carbon precipitation in the layer at high annealing temperatures as revealed by Raman and XRD analysis; this may further contribute to the lowering of the hardness of the material. This is because; the higher the carbon content the lower the hardness of the ZrC layer.

3.4. Surface morphology of as-deposited and annealed ZrC layers

Fig. 9 shows the SEM images of the ZrC samples annealed at 1500 °C, 1600 °C, 1700 °C and 1800 °C. The SEM image of the as deposited ZrC sample (1400 °C) has been included for comparison purposes. The SEM image of the as-deposited sample is composed of small grains which agglomerated to form clusters. The sample surface was rough and a number of voids were visible between the clustered crystals. The observable change in surface morphology of the sample after annealing at 1500 °C and 1600 °C was very little with respect to the as deposited sample. At annealing temperature of 1500 °C the presence of voids in between the clustered particles was still visible, except that at 1600 °C the number and size of the voids slightly decreased; the void looks shallower than at 1500 °C.

Annealing further at 1700 °C showed the absence of voids in between the clustered particles. The clustered grains combined to form bigger grains, thus the no voids between the particles are observed. At 1800 °C the hills and valleys between clustering were observed to decrease in height and depth causing them to be shallow. The surface seems to be less rough when compared to the lower annealing temperatures, this may be due to agglomeration and coalescence of the particles. Increase in the crystal size was explicitly observed at 1800 °C. The void between the clustered particles closed due to increased crystallite size and grain boundary migrations. The average crystallite size calculated from the XRD (using Scherrer's equation) and size of particles observed from the SEM micrographs both increased with annealing temperature. However, these two sets of results may not necessarily be compared because of the coalescence of crystallites into aggregates which depends on various crystal growth mechanisms. SEM provides information about the sample surface whereas XRD provides information of related to the volume of the sample.

4. Conclusion

In this study, we reported on the effect of annealing temperature on morphology, structural properties and hardness of ZrC layers. ZrC layers were grown on graphite substrates by chemical vapour deposition from methane and $ZrCl_4$ in the presence of argon and hydrogen gases at 1400 °C for 2 h at atmospheric pressure. The as-deposited ZrC layers were annealed from 1500 to 1800 °C for 2 h in vacuum (10^{-7} mbar). The XRD results showed the formation of ZrC and some traces of free carbon in the as-deposited samples. There was a general increase in average crystallite size with increasing annealing temperatures. There was a slight decrease in the diffraction angles with annealing temperature due to increase in lattice parameter values. The lattice strain and dislocation density decreased with annealing temperature; this may be due to decrease in lattice imperfection resulting from decreased concentration of grain boundaries. There were changes in the texture coefficient values, revealing changes in the preferred orientation of the crystallographic planes with annealing temperature. The crystallographic plane (111) was the less favoured orientation, whereas (200) and (220) were more favoured planes. Because of the carbon

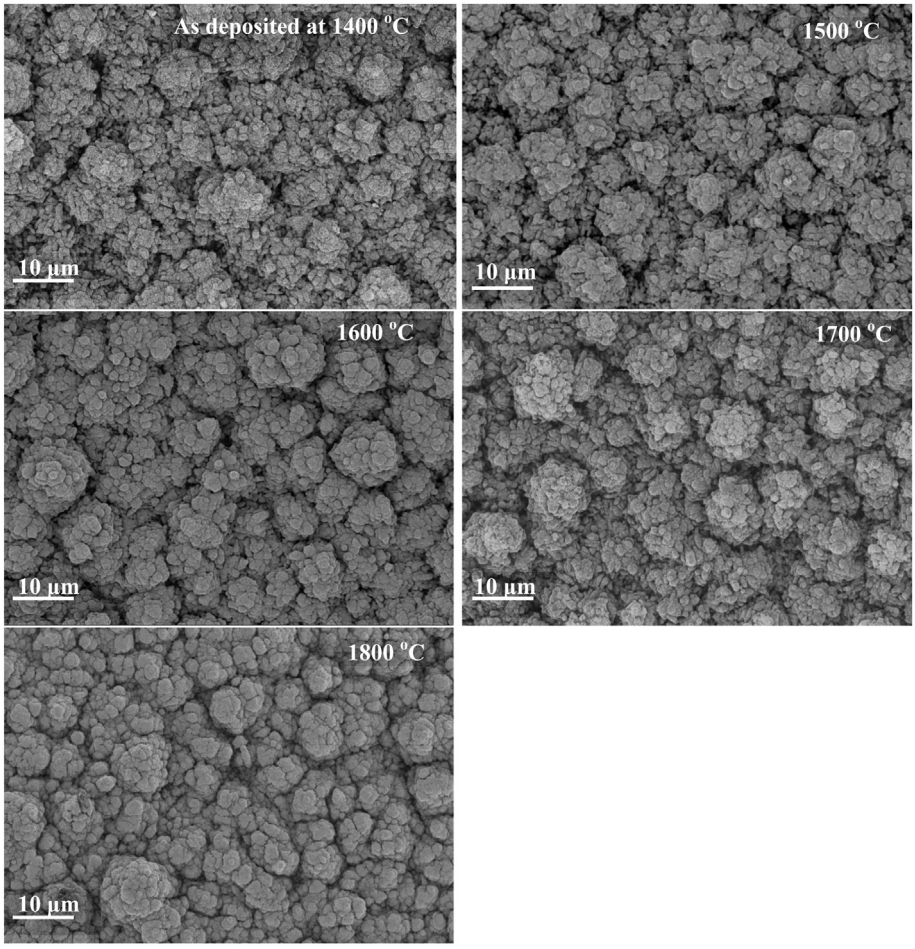

Fig. 9. Effect of annealing temperature on the surface morphology of ZrC layers.

inclusions in the as deposited samples, the Raman spectra revealed the presence of D and G peaks. The FWHM and the ratio I_D/I_G decreased with annealing temperature, implying that the carbon was becoming more crystalline and the defects in the carbon material were reducing. The hardness of the layers was observed to decrease with annealing temperature from 26.4 ± 0.6 GPa to 21.3 ± 0.5 GPa. At the deposition temperature of 1400 °C, the ZrC layer had small crystals clustered together surrounded by voids. The voids were annealed out at 1800 °C. With increase in annealing temperature the crystals increased in size and became more dense and coarse. The clustering and aggregating of particles into big agglomerates was more enhanced at 1800 °C. It was observed that increasing the annealing temperature had a significant effect on the microstructures and morphology of the CVD ZrC layers. This suggests that the as-deposited CVD ZrC layers should be annealed for long time at temperatures equal or higher than the temperature of the environment of their applications before use to stabilize the microstructures.

Declaration of competing interest

The authors declare that they have no competing interests.

CRediT authorship contribution statement

Saphina Biira: Conceptualization, Formal analysis, Investigation, Methodology, Writing - original draft. **T.T. Thabethe:** Investigation, Methodology, Writing - original draft. **T.T. Hlatshwayo:** Conceptualization, Supervision, Writing - review & editing. **H. Bissett:** Methodology, Resources, Supervision. **T. Ntsoane:** Formal analysis, Methodology. **J.B. Malherbe:** Resources, Supervision, Writing - review & editing.

Acknowledgements

The South African Nuclear Energy Corporation (Necsa) and the University of Pretoria (where CVD growth and characterisation of ZrC samples was conducted) are highly appreciated. The support from Busitema University which facilitated the writing of the manuscript is highly acknowledged.

References

[1] Y. Zhong, X. Xia, F. Shi, J. Zhan, J. Tu, H.J. Fan, Transition Metal Carbides and Nitrides in Energy Storage and Conversion, 2016, https://doi.org/10.1002/advs.201500286.
[2] C. Musa, R. Licheri, R. Orrù, G. Cao, D. Sciti, L. Silvestroni, L. Zoli, A. Balbo, L. Mercatelli, M. Meucci, E. Sani, Processing, mechanical and optical properties of additive-free ZrC ceramics prepared by Spark Plasma Sintering, Materials 9 (2016) 1–16, https://doi.org/10.3390/ma9060489.
[3] R.W. Harrison, W.E. Lee, Processing and properties of ZrC, ZrN and ZrCN ceramics: a review, Adv. Appl. Ceram. 115 (2016) 294–307.
[4] Y. Yang, C.A. Dickerson, H. Swoboda, B. Miller, T.R. Allen, Microstructure and mechanical properties of proton irradiated zirconium carbide, J. Nucl. Mater. 378 (2008) 341–348, https://doi.org/10.1016/j.jnucmat.2008.06.042.
[5] Y. Katoh, G. Vasudevamurthy, T. Nozawa, L.L. Snead, Properties of zirconium carbide for nuclear fuel applications, J. Nucl. Mater. 441 (2013) 718–742.
[6] S. Ueta, J. Aihara, K. Sawa, A. Yasuda, M. Honda, N. Furihata, Development of high temperature gas-cooled reactor (HTGR) fuel in Japan, Prog. Nucl. Energy 53 (2011) 788–793.
[7] M.A. Fütterer, L. Fu, C. Sink, S. De Groot, M. Pouchon, Y. Wan, F. Carré, Y. Tachibana, Status of the very high temperature reactor system, Prog. Nucl. Energy 77 (2014) 266–281, https://doi.org/10.1016/j.pnucene.2014.01.013.
[8] S. Biira, P.L. Crouse, H. Bissett, B.A.B. Alawad, T.T. Hlatshwayo, J.T. Nel, J.B. Malherbe, Optimisation of the synthesis of ZrC coatings in a radio frequency induction-heating chemical vapour deposition system using response surface methodology, Thin Solid Films 624 (2017) 61–69, https://doi.org/10.1016/j.tsf.2017.01.018.
[9] S. Biira, P.L. Crouse, H. Bissett, T.T. Hlatshwayo, E.G. Njoroge, J.T. Nel, T.P. Ntsoane, J.B. Malherbe, The role of ZrCl4 partial pressure on the growth characteristics of chemical vapour deposited ZrC layers, Ceram. Int. 43 (2017) 15133–15140, https://doi.org/10.1016/j.ceramint.2017.08.042.
[10] J.-H. Park, C.-H. Jung, W.-J. Kim, D.-J. Kim, J.-Y. Park, Microstructure and hardness changes of the CVD-ZrC film with different deposition temperature, J. Korean Ceram. Soc. 45 (2008) 567–571.
[11] Q.M. Liu, L.T. Zhang, Z.X. Meng, L.F. Cheng, Chemical vapor deposition (CVD) of ZrC coatings from ZrCl4-C3H6-H2, Adv. Mater. Res. (2011) 648–652.
[12] B.R. Kang, H.S. Kim, P.Y. Oh, J.M. Lee, H.I. Lee, S.M. Hong, Characteristics of ZrC barrier coating on SiC-coated carbon/carbon composite developed by thermal spray process, Materials 12 (2019) 747.
[13] S. Biira, P.L. Crouse, H. Bissett, T.T. Hlatshwayo, J.H. van Laar, J.B. Malherbe, Design and fabrication of a chemical vapour deposition system with special reference to ZrC layer growth characteristics, J. South. African Inst. Min. Metall. 117 (2017) 931–938, https://doi.org/10.17159/2411-9717/2017/v117n10a2.
[14] A.X.S. Bruker, TOPAS, Version 4.2, Bruker AXS, Karlsruhe, Ger, 2009.
[15] K. Venkateswarlu, A.C. Bose, N. Rameshbabu, X-ray peak broadening studies of nanocrystalline hydroxyapatite by Williamson-Hall analysis, Phys. B Condens. Matter 405 (2010) 4256–4261.
[16] R.R. Triloki, T.B.K. Singh, X-ray diffraction line profile analysis of KBr thin films, Appl. Phys. A 122 (2016) 1–11, https://doi.org/10.1007/s00339-016-0293-3.
[17] L. Hosseinzadeh, J. Baedi, A.K. Zak, X-ray peak broadening analysis of Fe50Ni50 nanocrystalline alloys prepared under different milling times and BPR using size strain plot (SSP) method, Bull. Mater. Sci. 37 (2014) 1147–1152.
[18] V.D. Mote, Y. Purushotham, B.N. Dole, Williamson-Hall analysis in estimation of lattice strain in nanometer-sized ZnO particles, J. Theor. Appl. Phys. 6 (2012) 1–8.
[19] M. Ermrich, D. Opper, XRD for the Analyst: Getting Acquainted with the Principles, PANalytical, Eindhoven, 2013.
[20] V.S. Vinila, R. Jacob, A. Mony, H.G. Nair, S. Issac, S. Rajan, A.S. Nair, J. Isac, XRD studies on nano crystalline ceramic superconductor PbSrCaCuO at different treating temperatures, Cryst. Struct. Theor. Appl. 3 (2014) 1–9.
[21] B.D. Cullity, S.R. Stock, Elements of X-Ray Diffraction, first ed., Addison-Wesley Publishing company Inc, Massachusetts, 1956.
[22] X. Wang, L. Hu, K. Liu, Y. Zhang, Grain growth kinetics of bulk AZ31 magnesium alloy by hot pressing, J. Alloys Compd. 527 (2012) 193–196, https://doi.org/10.1016/j.jallcom.2012.03.006.
[23] C. V Thompson, Structure evolution during processing of polycrystalline films, Annu. Rev. Mater. Sci. 30 (2000) 159–190.
[24] C.-C. Liu, J.-H. Huang, C.-S. Ku, S.-J. Chiu, J. Ghatak, S. Brahma, C.-W. Liu, C.-P. Liu, K.-Y. Lo, Crystal orientation dynamics of collective Zn dots before preferential nucleation, Sci. Rep. 5 (2015) 12533, https://doi.org/10.1038/srep12533.
[25] Y. Wang, Q. Liu, J. Liu, L. Zhang, L. Cheng, Deposition mechanism for chemical vapor deposition of zirconium carbide coatings, J. Am. Ceram. Soc. 91 (2008) 1249–1252, https://doi.org/10.1111/j.1551-2916.2007.02253.x.
[26] N. Moelans, B. Blanpain, P. Wollants, Pinning effect of second-phase particles on grain growth in polycrystalline films studied by 3-D phase field simulations, Acta Mater. 55 (2007) 2173–2182, https://doi.org/10.1016/j.actamat.2006.11.018.
[27] R. Sharma, D.P. Bisen, U. Shukla, B.G. Sharma, X-ray diffraction: a powerful method of characterizing nanomaterials, Recent Res. Sci. Technol. 4 (2012) 77–79.
[28] J.P. Enríquez, X. Mathew, Influence of the thickness on structural, optical and electrical properties of chemical bath deposited CdS thin films, Sol. Energy Mater. Sol. Cells 76 (2003) 313–322.
[29] C. V Thompson, R. Carel, Stress and grain growth in thin films, J. Mech. Phys. Solid. 44 (1996) 657–674.
[30] S. Aksoy, Y.Y.Y. Caglar, S. Ilican, M. Caglar, Effect of deposition temperature on the crystalline structure and surface morphology of ZnO films deposited on p-Si, Adv. Control. Chem. Eng. Civ. Eng. Mech. Eng. (2010) 227–231.
[31] G.K. Williamson, R.E. Smallman III., Dislocation densities in some annealed and cold-worked metals from measurements on the X-ray debye-scherrer spectrum, Philos. Mag. A 1 (1956) 34–46.
[32] D.N. Lee, Current understanding of annealing texture evolution in thin films and interconnects, Z. Metallkd. 96 (2005) 259–268.
[33] K.S. Munir, M. Qian, Y. Li, D.T. Oldfield, P. Kingshott, D.M. Zhu, C. Wen, Quantitative analyses of MWCNT-Ti powder mixtures using Raman spectroscopy: the influence of milling parameters on nanostructural evolution, Adv. Eng. Mater. 17 (2015) 1660–1669, https://doi.org/10.1002/adem.201500142.
[34] D. Kim, Y.B. Chun, M.J. Ko, H. Lee, M. Cho, J.Y. Park, W. Kim, Microstructure evolution of a ZrC coating layer in TRISO particles during high-temperature annealing, J. Nucl. Mater. 479 (2016) 93–99, https://doi.org/10.1016/j.jnucmat.2016.06.024.
[35] S. Pellegrino, L. Thomé, A. Debelle, S. Miro, P. Trocellier, Radiation effects in carbides : TiC and ZrC versus SiC, Nucl. Instrum. Methods Phys. Res. B. 327 (2014) 103–107, https://doi.org/10.1016/j.nimb.2013.11.046.
[36] M. Patel, C.L.A. Ricardo, P. Scardi, P.B. Aswath, Morphology, structure and chemistry of extracted diesel soot—Part I: transmission electron microscopy, Raman spectroscopy, X-ray photoelectron spectroscopy and synchrotron X-ray diffraction study, Tribol. Int. 52 (2012) 29–39.
[37] A.C. Ferrari, D.M. Basko, Raman spectroscopy as a versatile tool for studying the properties of graphene, Nat. Nanotechnol. 8 (2013) 235–246.
[38] L.G. Cancado, A. Jorio, E.H.M. Ferreira, F. Stavale, C.A. Achete, R.B. Capaz,

M.V.O. Moutinho, A. Lombardo, T.S. Kulmala, A.C. Ferrari, Quantifying defects in graphene via Raman spectroscopy at different excitation energies, Nano Lett. 11 (2011) 3190–3196, https://doi.org/10.1021/nl201432g.

[39] S.N. Naik, The Hall – petch and inverse Hall – petch relations and the hardness of nanocrystalline metals, J. Mater. Sci. 55 (2020) 2661–2681, https://doi.org/10.1007/s10853-019-04160-w.